# DELIVERABLE REPORT

| | |
|---|---|
| **Deliverable no. / title:** | D3.1 Upgraded kMC model |
| **Lead beneficiary:** | CNRS - LRCS |
| **Nature of deliverable:** | |
| **Dissemination level:** | PU – Public |
| **Due date:** | M10 / October 2020 |

| | |
|---|---|
| **Grant Agreement number:** | 875489 |
| **Project acronym:** | SONAR |
| **Project title:** | Modelling for the search for new active materials for redox flow batteries |
| **Funding scheme:** | H2020-LC-BAT-2019 |
| **Coordinator:** | Fraunhofer ICT<br>Jens Noack<br>**Tel:** 0049 721 4640 870<br>**E-mail:** jens.noack@ict.fraunhofer.de |
| **Project website:** | www.sonar-redox.eu |

# Table of contents

1 Introduction ..... 3
2 KMC model description ..... 4
2.1 General assumptions ..... 4
2.2 Grid geometries ..... 5
2.3 Boundary conditions ..... 6
2.4 Basic events and rates calculation ..... 6
2.4.1 Diffusion event and diffusion rate ..... 6
2.4.2 Dimerization events ..... 7
2.4.3 Electrochemical reaction - discharging events ..... 8
3 EDL model and the impact on kMC kinetics ..... 8
3.1 Compact layer model ..... 9
3.2 Diffuse layer model ..... 13
4 Result and discussion ..... 15
5 Conclusions and perspectives ..... 18
6 References ..... 19

# 1 Introduction

This document describes the first version of the upgraded kinetic Monte Carlo (kMC) model which has been modified to be used for SONAR project. The objective of developing this kMC model is to simulate the electrochemical phenomenon inside the electrochemical double layer (EDL) region of a methyl viologen ($MV$)/4-hydroxy-2,2,6,6-tetramethylpiperidin-1-oxyl ($4-HO-TEMPO$) redox flow battery (RFB) system.

Kinetic Monte Carlo is a popular computational tool that solves complex systems with random numbers [1][2]. During the past few decades, it has been well applied to computational chemistry and material science due to its outstanding efficiency and simple versatility [3][4][5]. In this study, the algorithm that we used is the so-called Variable Step Size Method (VSSM) which is one of the most popular kMC algorithms. The process of a VSSM algorithm is listed as follows (Figure 1):

1) Define an initial state of the system with related conditions;
2) Search for all the possible event $i$ for the current state, and calculate the rate $k_i$ of each event;
3) Generate the first random number $\rho_1 \in (0,1)$ to choose and execute a possible event $j$ according to Eq.1;

$$\sum_{i=1}^{j-1} k_i < \sum_{i} k_i \rho_1 \leq \sum_{i=1}^{j} k_i \quad (1)$$

4) Generate the second random number $\rho_2 \in (0,1)$, and update the simulation clock by adding a time step $\Delta t$ (Eq. 2)

$$\Delta t = -\frac{\rho_2}{\sum k_i} \quad (2)$$

5) Check if the system meets the cut-off condition or not. If not, restart from step 2). If so, stop the simulation.

The model of Task 3.1 is originated from the previous work of a kMC model developed by our team [6], which simulates the semi-solid redox flow battery systems. This model considers the volume expansion of silicon particles during the discharging process and the dynamic electronic percolation networks induced by a suspension of carbon particles. The various particle diffusion rates are also considered by calculating the slurry's viscosity dynamically.

Based on that model, we implemented the impact of EDL and the calculation of reaction rates in the specific context of organic redox flow batteries. The following part of this report will introduce our model which is capable of simulating three types of events: molecular diffusion, electrochemical reaction (discharge) and formation of dimers, the latter being one ageing mechanism recognized to happen in the batteries under investigation here. Section 2 presents the calculation of these event rates without considering the EDL impact, which is discussed later in Section 3.

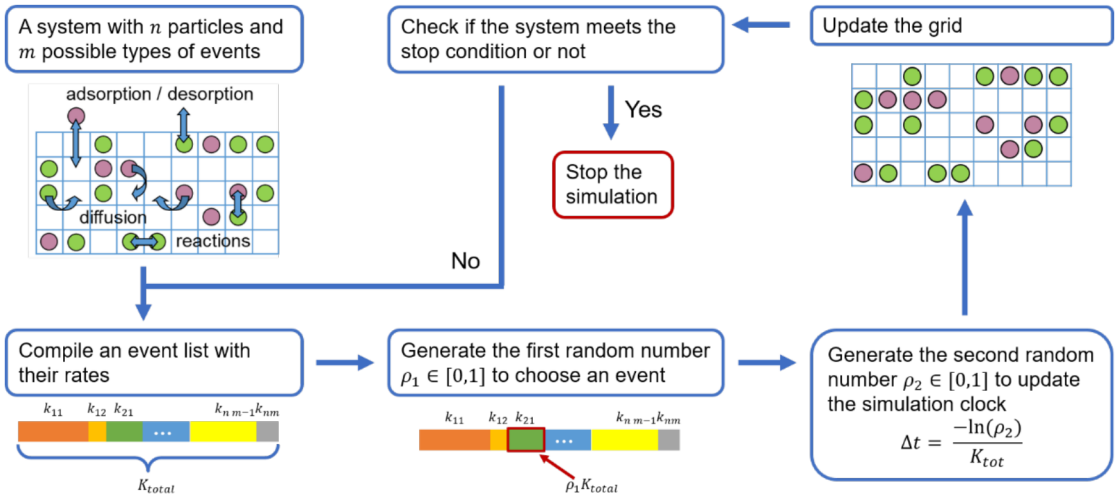


**Figure 1.** Computational workflow behind our kMC - VSSM algorithm.

# 2 KMC model description

## 2.1 General assumptions

The model presented in this report is based on the following assumptions:

- The system is simulated under isothermal conditions. The temperature fluctuation is not taken into consideration in this study;
- The electrode surface of the redox flow battery system is assumed to be flat;
- The cross-over effect is not considered. We assume the discharge process to be symmetrical, and our model focuses only on the negative electrode;
- The thickness of the EDL region is much smaller than the one of the boundary layers.

As the model is under development, more details, *i.e.* convection, membrane cross-over effect, would be included in the future version, providing a broader spectrum of dynamic factors to be explored through simulations.

## 2.2 Grid geometries

Our kMC model is supported on an "on-lattice" approach. We chose a cubic mesh to build the simulation grid. The mesh unit size was set to be 8 Å, which is similar to the solvated methyl viologen molecules modelled in BIOVIA Materials Studio [7]. Only solvated $MV^+$, $MV^{2+}$, $[MV]^0$ and $Cl^-$ are represented inside the grid. Each $MV^+$, $MV^{2+}$, $[MV]^0$ and $Cl^-$ occupies one grid unit. The size difference between methyl viologen molecules and chloride ions are neglected while building the mesh since the number of grid units is large enough to cover the target concentration.

On the other hand, all the molecules and ions sizes are respectively considered when encountering calculations. To simplify the computational process, we neglect their molecular shape, thus each considered molecule takes only one unit, and their rotations can be neglected. For those empty grid units, they were assumed to be fulfilled with water molecules and electrolyte ions which do not participate in the reaction. However, even if we do not represent them in the grid unit, their impact on the motion and reactions of the molecule is still captured by considering the Frumkin effect as it will be discussed later in this document.

The simulation box was separated into three parts to represent our EDL model, as shown in **Figure 2**. The electrode surface is located on the top of the simulation box. The thickness of the compact layer $d$ was set to 1.6 nm, which is also considered as the electronic tunnelling distance. The rest of the simulation box represents the diffuse layer. Outside the simulation box is the bulk which is not illustrated in **Figure 2**. The entire simulation box is a cube with a size of $8 \times 8 \times 15$ grid units on each side (length x width x height).

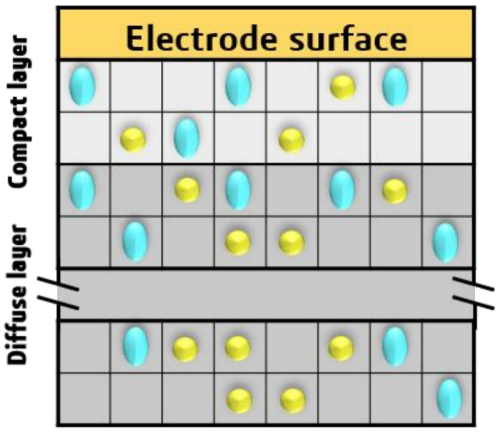


**Figure 2.** 2D schematic demonstration of the initial simulation grid arrangement. The light blue particles represent $MV^+$, and the yellow particles represent $Cl^-$ ions.

## 2.3 Boundary conditions

During operation, both the anolyte and the catholyte are stocked separately in external reservoirs and pumped through the cell stack to react. The electrolyte flow is assumed to be constant, and the back-flow is assumed to be negligible. While the electrolyte flowing through the reactor, the oxidation of $MV^+$ takes place in anolyte. $Cl^-$ transfer across the membrane to balance the charge.

In this work, we have aimed to simulate the galvanostatic discharging process of a low concentration electrolyte system where the initial concentration of $MV^+$ is set at 0.2 M. The initial concentration range can be expanded to 1.5 M with future modelling development, which is the typical concentration used in large scale Redox Flow Batteries [8].

The simulation lattice in our model represents only the EDL region with periodic boundary conditions. While discharging, the material balance and the charge balance inside the simulation grid are expressed respectively by Eq. 3 and Eq. 4

$$\frac{dc_{MV^{2+}}}{dt} = -\frac{dc_{MV^{+}}}{dt} \tag{3}$$

$$c_{MV^{2+}} = 2c_{MV^{2+}} + c_{MV^{+}} - c_{Cl^{-}} \tag{4}$$

where $c_{MV^+}$ is the concentration of $MV^+$, $c_{MV^{2+}}$ is the concentration of $MV^{2+}$ and $c_{Cl^-}$ is the concentration of $Cl^-$. Outside the simulation box is the bulk of electrolyte where the charge neutrality is kept during the whole discharging process.

## 2.4 Basic events and rates calculation

### 2.4.1 Diffusion event and diffusion rate

As we assume the EDL region is inside the boundary layer, the convection due to the supply flow is neglected, and the main molecular displacement considered in this work is diffusion. Diffusion is generated only by translation with a step size equalling to the mesh size, and no overlapping in the grid is tolerated. All the considered species are assumed to be mobile except $[MV]^0$ due to its insolubility.

The diffusion rate $K_{diff}$ is measured by Eq. 5 and the diffusion coefficient $D_{diff}$ is expressed by the Stokes-Einstein equation as presented in Eq. 6, where $k_B$ is the Boltzmann constant, $T$ is the system's absolute temperature, $\mu$ is the dynamic viscosity of the negolyte, $r$ is the

hydrodynamic radius of the considered species $i$ and $A$ is the cross-sectional surface area of the considered species [3][4]

$$K_{diff} = \frac{D_{diff}}{A} \tag{5}$$

$$D_{diff} = \frac{k_B T}{6\pi\mu r_i} \tag{6}$$

The Stokes-Einstein equation takes the dynamic viscosity of the electrolyte and the molecule's size into consideration. By substituting the corresponding values of $MV^+$ and $MV^{2+}$, we obtained the calculated diffusion coefficient around $2 \times 10^{-6}\ cm^2/s$ which is similar to the value extracted from experimentations for low concentration methyl viologen electrolyte [10].

### 2.4.2 Dimerization events

According to Hu *et al.* [11], the capacity loss of the methyl viologen based negolyte is mainly caused by the polymerizations. A general formation of dimers and some trimers and quadrimers formation have been observed for a low concentration anolyte (0.1 M). For a high concentration case, 1M or higher, it is reasonable to expect a formation of n-mers [12].

This phenomenon is also included in our model to study further the degradation of the target ORFB system. In this work, we focus only on the dominant degradation effect of lower concentration case, the dimerization. It is believed that a disproportionation reaction often follows the formation of dimers and generates a $MV^{2+}$ and a $[MV]^0$. The later one is insoluble and will precipitate out [12].

In our model, the dimerization event is generated when two $MV^+$ locate in neighbouring grid units. The produced dimers are assumed to decompose immediately and end into a $MV^{2+}$ and a $[MV]^0$. The dimerization kinetics is described by a constant $K$ (Eq. 7) extracted from the previous work of Liu *et al.* [10]. They explored a full-cell cycling test using 4-HO-TEMPO as catholyte. The cycling condition was 0.5 M $MV^+$ and 0.5 M *4-HO-TEMPO* with 1.5 M *NaCl* as supporting salt. The input current density was 60 mA/cm$^2$. Their work pointed out that the capacity retention rate of a full-cell system is overall 99% per cycle which will be lower when increasing the electrolyte concentration.

$$\begin{aligned} K_{dimers} &= K, \quad if\ two\ MV^+\ are\ next\ to\ each\ other \\ K_{dimers} &= 0, \quad other\ situations \end{aligned} \tag{7}$$

### 2.4.3 Electrochemical reaction - discharging events

The objective of this work is to study the electrochemical kinetics of the methyl viologen system. Our target electrochemical reaction is the oxidation of $MV^+$. This discharging event only takes place inside the electronic tunnelling distance, which is considered to be the same value as the thickness of the compact layer.

The discharging kinetics is described by the Eyring's expression from the Transition-State-Theory. Previous work by our group [8][9] pointed out the term $E_\lambda$ in the equation needed to be corrected by adding the $f(\sigma)$ term which is a function of the electrode surface charge density $\sigma$. The calculation of $f(\sigma)$ is explained in details in the next section of the report. $E_\lambda$ is the reorganization energy of the electron transfer process from the Marcus' theory which can be obtained through Density Functional Theory (DFT) calculations. The reorganization energy captures the free energy barrier of the electron transfer in the electrolyte.

After the correction, the reaction rate is expressed as Eq. 8:

$$K_{dis} = \kappa_0 \frac{k_B T}{h} \exp\left(\frac{-E_\lambda \mp f(\sigma)}{RT}\right) \tag{8}$$

where $\kappa_0$ stands for the vibrational frequency of the transition state. $h$ and $R$ are the Planck constant and the ideal gas constant. $-E_\lambda \mp f(\sigma)$ is noted as the effective reorganization energy (the sign depends on whether the occurring reaction is oxidation or reduction).

# 3 EDL model and the impact on kMC kinetics

Similarly to the classical Gouy-Chapman-Stern theory [15], our EDL model consists of a compact layer fulfilled by solvent molecules and ions (adsorbed or not) and a diffuse layer where the concentration of the oppositely charged ions decreases along with the distance from the surface. The geometry structure of the EDL is shown in **Figure 3**.

The length of the EDL region is measured as the Debye length $\lambda_D$ and is calculated by the following equation:

$$\lambda_D = \sqrt{\frac{\varepsilon_0 \varepsilon_{DL} k_B T}{\sum_i c_0^i (z_i e)^2}} \tag{9}$$

In Eq. 9, $\varepsilon_0$ is the electric permittivity of vacuum. $\varepsilon_{DL}$ is the relative electric permittivity of the bulk electrolyte. $e$ is the elementary charge. $c_0^i$ and $z_i$ are respectively the concentration and the valence of related species $i$. By substituting the corresponding values of methyl viologen electrolytes, we obtained the Debye length $\lambda_D$, which is around 10 nm and varies slightly with different states of charge.

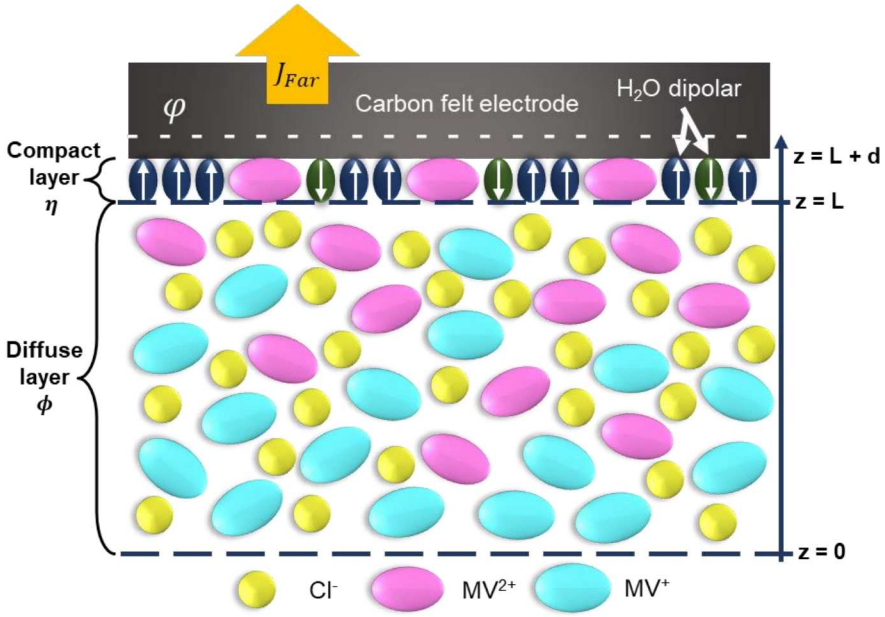


**Figure 3.** Schematic illustration of the EDL structure. The thickness of the diffuse layer is $\boldsymbol{L}$. The thickness of the compact layer is $\boldsymbol{d}$. Oriented water dipoles are indicated with arrows.

The previous research by our group [16] indicated that the electrostatic potential of the rigid electrode surface $\varphi$ is calculated by the sum of the electrostatic potential outside the compact layer $\phi_L$ (potential at the interface between the compact layer and the diffuse layer) and the potential drop $\eta$ between the electrode and the electrolyte (Eq. 10).

$$\varphi = \phi_L + \eta \tag{10}$$

### 3.1 Compact layer model

To calculate the potential drop $\eta$ through the compact layer, we consider it as the sum of two different potential drops, $\triangle \eta_1$ and $\triangle \eta_2$. $\triangle \eta_1$ is the potential drop related to the thickness of the compact layer and the charge density on the electrode surface $\sigma$. $\triangle \eta_2$ is the potential drop related to the adsorbed species charge density $\Gamma$, which is also a function of $\sigma$. In the present work, we

only consider the adsorbed water dipoles, while more related absorbable species will be included in the future work when DFT calculations in this respect will be performed in WP 2.

The charge density on the electrode surface $\sigma$ is expressed through the input current density $J_{inp}$ and the Faradaic current density $J_{Far}$ as shown in Eq. 11:

$$J_{inp} - J_{Far} = -\frac{\partial \sigma}{\partial t} \tag{11}$$

The Faradaic current density $J_{Far}$ is generated by the oxidation reaction on the electrode surface and calculated through Eq. 12 where $\Delta Q$ is the total charge transferred by all the electrochemical reaction events. $S$ is the electrode surface, and $\Delta t$ is the total simulation time.

$$J_{Far} = \frac{\Delta Q}{S \Delta t} \tag{12}$$

The value of charge density on the electrode surface $\sigma$ impacts both potential drops, $\triangle \eta_1$ and $\triangle \eta_2$, which then affects the discharging kinetics. The first potential drop $\triangle \eta_1$ is expressed through Eq. 13 where $\varepsilon_{CL}$ is the relative electric permittivity of the compact layer:

$$\triangle \eta_1 = \frac{\sigma d}{\varepsilon_0 \varepsilon_{CL}} \tag{13}$$

The adsorbed water dipole charge density $\Gamma(\sigma)$ is related to a layer of punctual water dipoles. The dipolar surface density $\Gamma$ depends on the number of water dipoles per unit area and their orientations (Eq. 14):

$$\Gamma = p(\vec{n} - \overleftarrow{n}) \tag{14}$$

To simplify the simulations, we divided all the adsorbed water dipoles into two categories, those pointing towards the electrode and those pointing towards the electrolyte. In Eq. 14, $\vec{n}$ and $\overleftarrow{n}$ refer to the number of water dipoles per unit area of these two categories respectively. $p$ is the dipolar moment of a water molecule.

We denote $n_{max}$ as the maximum number of available sites per unit area which leads us to the following relation

$$\vec{n} + \overleftarrow{n} + n_{free} = n_{max} \tag{15}$$

where $n_{max} = \frac{1}{{d_m}^2}$, $d_m$ is the thickness of a water molecule, and $n_{free}$ is the number of free sites per unit area.

By applying the law of mass action and considering the adsorbed water dipoles orientations, the surface adsorption equilibrium reactions are expressed in Eq. 16 and Eq. 17 with their corresponding activation energy $\Delta\vec{G}_{H_2O}$ and $\Delta\overleftarrow{G}_{H_2O}$

$$\vec{n} = \Theta_{H_2O} n_{free} \exp\left(\frac{-\Delta\vec{G}_{H_2O}}{RT}\right) \tag{16}$$

$$\overleftarrow{n} = \Theta_{H_2O} n_{free} \exp\left(\frac{-\Delta\overleftarrow{G}_{H_2O}}{RT}\right) \tag{17}$$

where $\Theta_{H_2O}$ is the water surface fraction on the electrode surface (dimensionless).

Following the previous theory of our group [16], the activation energy term can be separated into three distinct terms:

$$\Delta G_{H_2O} = \Delta G_{H_2O}^{chem} + \Delta G_{H_2O}^{elec} + \Delta G_{H_2O}^{inter} \tag{18}$$

where $\Delta G_{H_2O}^{chem}$ is the chemical adsorption energy assumed to be constant and independent of the dipolar orientation (Eq. 19). $\Delta G_{H_2O}^{elec}$ is the electrostatic energy related to the work of electrical field to carry a dipole from infinite distance to the electrode surface. $\Delta G_{H_2O}^{inter}$ is the interpolar interaction energy. The latter two terms are odd functions of the adsorption directions as expressed in Eq. 20 and Eq. 21.

$$\Delta\vec{G}_{H_2O}^{chem} = \Delta\overleftarrow{G}_{H_2O}^{chem} = \Delta G_{H_2O}^{chem} \tag{19}$$

$$\Delta\vec{G}_{H_2O}^{elec} = -\Delta\overleftarrow{G}_{H_2O}^{elec} \tag{20}$$

$$\Delta\vec{G}_{H_2O}^{inter} = -\Delta\overleftarrow{G}_{H_2O}^{inter} \tag{21}$$

Therefore, based on the adsorbed dipole's orientation, we have the activation energy of both adsorption reactions (Eq. 22 and Eq. 23):

$$\Delta\vec{G}_{H_2O} = \Delta\vec{G}^{chem}_{H_2O} + \Delta\vec{G}^{elec}_{H_2O} + \Delta\vec{G}^{inter}_{H_2O} \quad (22)$$

$$\Delta\overleftarrow{G}_{H_2O} = \Delta\vec{G}^{chem}_{H_2O} - \Delta\vec{G}^{elec}_{H_2O} - \Delta\vec{G}^{inter}_{H_2O} \quad (23)$$

According to the previous work of our group [13], the electrostatic energy and the interaction energy can be calculated through Eq. 24 and Eq. 25:

$$\Delta\vec{G}^{elec}_{H_2O} = \frac{N_A p\sigma}{\varepsilon_0\varepsilon_{CL}} \quad (24)$$

$$\Delta\vec{G}^{inter}_{H_2O} = \frac{\xi[3]N_A p^2}{2\pi\varepsilon_0\varepsilon_{DL}d_m}(\vec{n} - \overleftarrow{n}) \quad (25)$$

where $N_A$ is the Avogadro constant. $\xi[3]$ is Riemann Zeta-function which equals to 1.202. To simplify the notation, we combine $\Delta\vec{G}^{elec}_{H_2O}$ and $\Delta\vec{G}^{inter}_{H_2O}$ and denote $X_i$ as:

$$X_{H_2O} = \frac{\Delta\vec{G}^{elec}_{H_2O} + \Delta\vec{G}^{inter}_{H_2O}}{RT} \quad (26)$$

After the combination of Eq. 16 - Eq.18, Eq. 22 - Eq. 25, we have the expression of $X_{H_2O}$, which is a transcendental equation as follows:

$$X_{H_2O} = b\sigma + \frac{a\cdot c\cdot\sinh(-X_{H_2O})}{{d_m}^2(1 + a\cdot\cosh(X_{H_2O}))}$$

$$with\ a = 2\Theta_{H_2O}\exp\left(\frac{-\Delta\vec{G}^{chem}_{H_2O}}{RT}\right), b = \frac{p}{k_B T\varepsilon_0\varepsilon_{CL}}, c = \frac{\xi[3]p^2}{2\pi k_B T\varepsilon_0\varepsilon_{DL}d_m} \quad (27)$$

Eq. 14 then becomes

$$\Gamma(\sigma) = \frac{a\cdot p\cdot\sinh(-X_{H_2O})}{{d_m}^2(1 + a\cdot\cosh(X_{H_2O}))} \quad (28)$$

Therefore, $\triangle\eta_2$ is calculated through

$$\triangle\eta_2 = \frac{\Gamma(\sigma)}{\varepsilon_0\varepsilon_{DL}} \quad (29)$$

By substituting the values of $\triangle \eta_1$ and $\triangle \eta_2$, we obtain the total potential drop $\eta$ through the compact layer, which impacts the electrochemical kinetics through the $f(\sigma)$ term (Eq. 30):

$$f(\sigma) = \alpha F\eta = \alpha F\left(\frac{\sigma d}{\varepsilon_0 \varepsilon_{CL}} + \frac{\Gamma(\sigma)}{\varepsilon_0 \varepsilon_{DL}}\right) \tag{30}$$

$\alpha$ is a pre-factor which signifies the equilibrium state of the reaction, and $F$ is the Faraday constant.

### 3.2 Diffuse layer model

The calculation of the electric potential $\phi$ and the electric field $E$ within the diffuse layer was carried out by integrating a solver for the Poisson equation within the kMC simulation. Concretely, the Poisson equation is defined as:

$$\nabla^2 \phi = -\frac{\rho}{\varepsilon_0 \varepsilon_{DL}} \tag{31}$$

where $\rho$ is the volume charge density.

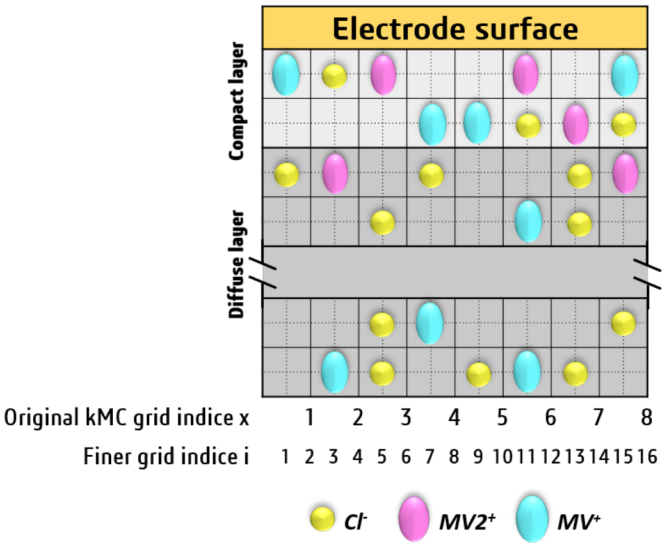


**Figure 4.** Illustration of the indices of the finer grid for Poisson equation and the indices of the kMC grid. The relation between the two different indices are as follows: $\boldsymbol{i = 2x - 1;\ j = 2y - 1;\ k = 2z - 1.}$

This differential equation is then solved using the Finite Difference Method on a finer cubic grid with indices $i$, $j$ and $k$, composed of even subdivisions of the original grid used for the kMC

as shown in **Figure 4**, such that the particle centres in the original grid always lie on top of the grid points used for solving Eq. 31. We approximate the $MV^{+}$, $MV^{2+}$ and $MV^{-}$ as point charges, therefore the charge density is defined as

$$\rho(\boldsymbol{r}) = \sum_{i=1}^{N} ez_i \delta(\boldsymbol{r} - \boldsymbol{r_i}) \tag{32}$$

where $\delta$ is the Dirac delta function.

The boundary conditions employed for solving the Poisson equation in a simulation box with dimensions $L_x, L_y, L_z$, are the following:

1) Dirichlet boundary conditions: $\phi_{ij0} = 0$, simulating the reference potential at the bulk electrolyte;
2) Neumann boundary conditions: $\left.{}^{\partial\phi}/_{\partial z}\right|_{ijL_z} = {}^{\sigma}/_{\varepsilon_0 \varepsilon_{DL}}$.
3) Periodic boundary conditions at $i = j = 0$, $i = L_x$, and $j = L_y$

The discretization of Eq. 31 leads to a system of linear equations

$$A \cdot x = b \tag{33}$$

where $A$ is the coefficient matrix containing the linear relationship between the electric potential and the charge density, $\boldsymbol{x}$ is a flattened vector containing the values of the electric potential at grid points $i, j,$ and $k$, and $\boldsymbol{b}$ contains the information about the charge density and the boundary conditions. Direct solution by inversion of matrix $\boldsymbol{A}$ is possible; however, it is important to realize that, by construction, matrix $\boldsymbol{A}$ is sparse. We can then take full advantage of the SciPy [17] sparse solvers for an almost tenfold performance boost, which is critical, given that Eq. 33 is going to be solved once per kMC iteration, and it is therefore important to avoid big bottlenecks.

By calculating the gradient of the electrical potential $\phi$ inside the diffuse layer, we obtain the electrical field distribution at each grid nodes of the diffuse layer

$$\boldsymbol{E_{(i,j,k)}} = -\boldsymbol{\nabla}\phi_{(i,j,k)} \tag{34}$$

The electrical field generated by the EDL structure influences the displacement of the concerned particles by migration. To include this mechanism, we describe the migration and the diffusion together by considering the initial diffusion rate as the hopping rate and adding the

Arrhenius type expression of the electrical field jumping frequency impact which is shown in Eq. 35 [18]:

$$K_{hop} = K_{diff}\, exp\left(\frac{\pm zerE_{(x,y,z)}}{k_B T}\right) \tag{35}$$

The numerator of the exponential term is the needed electrical field work to generate the hopping event. The value of the electrical field $E_{(x,y,z)}$ in Eq. 35 corresponds to the position of each displaceable particle position on the simulation grid. The '$\pm$' sign depends on the charge carried by the concerned particle, the hopping direction and the electrical field direction. For example, when considering a hopping event along the electrical field direction of a positively charged particle, the electrical field assists the hopping event and increases the hopping rate. While an opposite hopping direction is unfavourable by the electrical field and the hopping rate will decreased.

# 4 Result and discussion

In this work, we simulate the anolyte system under galvanostatic conditions. The initial concentration of the $MV^+$ electrolyte was set at 0.2 M, with a 100% state of charge. We assume the reference electrode is NHE. The results are shown below. **Figure 5** (a) and (b) are respectively, the concentration and the potential evolution during the discharging process.

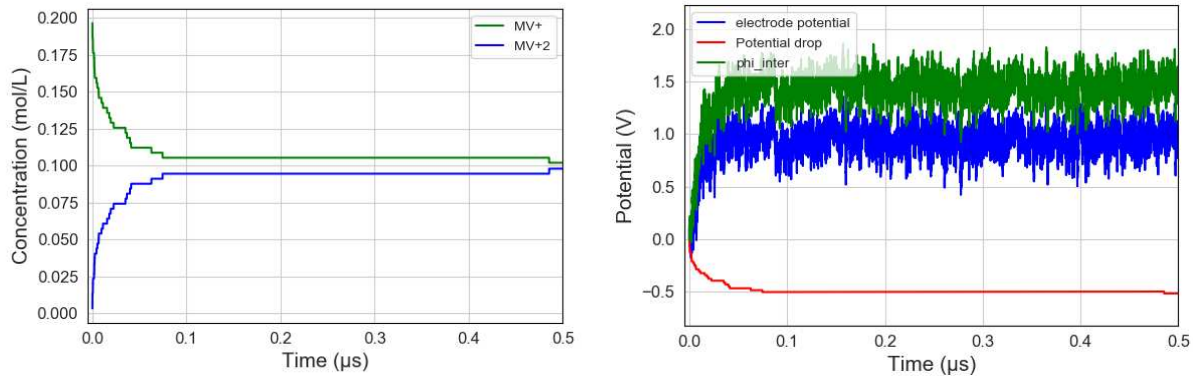


(a) (b)

**Figure 5.** (a) Calculated concentration evolution during a galvanostatic process; (b) Calculated potential evolution during a galvanostatic discharging process.

At the beginning of the discharging process, the electrochemistry dominates the system dynamics, and a large number of electrochemical reactions occur. With the discharging of $MV^+$, negative charges accumulate on the electrode, and the positive charges accumulate inside the EDL region. This fact creates an electrostatic field pointing to the electrode inside the EDL region, which impacts the electrochemical reactions and the molecules motions.

As shown in **Figure 5**, during the whole discharging process, the potential drop $\eta$ remains negative and keep decreasing. According to Eq. 8, the decreasing potential drop $\eta$ slows down the electrochemical kinetics and leads the system into a relatively steady state where molecule displacement dominates the system dynamics until the end of the simulation. As we set the dimerization rate at a relatively low value, the formation of dimers is not yet observed from the results.

**Figure 6** presents four configurations from different states of charge levels, which demonstrates the migration dominated molecule motions. As shown in the figure, positively charged molecules ($MV^+$ and $MV^{2+}$) move towards the electrode surface, and the negatively charged particles are repelled from it. As the discharge progresses, the electric field becomes stronger, which attracts more positive charged particles approaching the electrode surface.

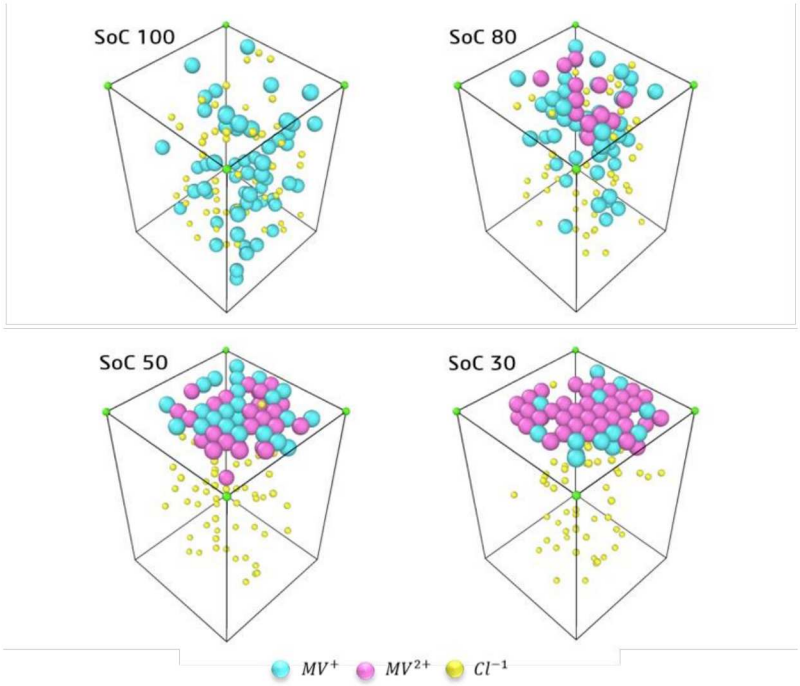


**Figure 6.** Calculated particle distribution along the discharging process (dimerization events are not activated).

We intend to upscale the simulation to provide effective electrochemical quantities as lumped factors to the continuum models developed in WP 4. The first lumped factor is the equivalent capacitance of the EDL region $C_{eq}$ which is calculated through

$$J_{inp} - J_{Far} = C_{eq}\left(\frac{d(\eta + \phi_L)}{dt}\right) \tag{36}$$

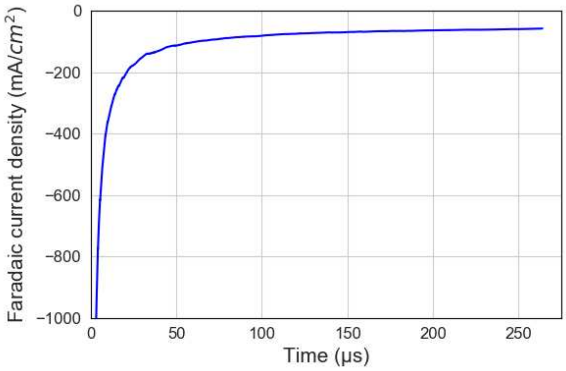


**Figure 7.** Faradaic current density evolution

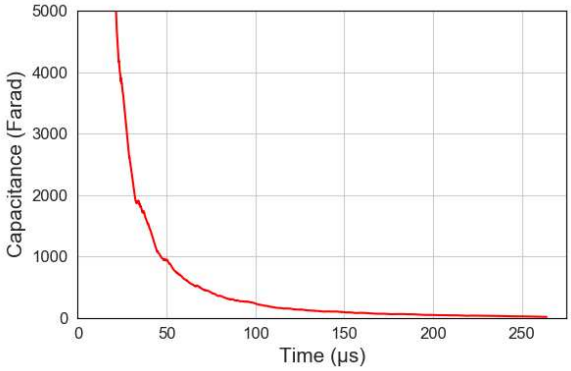


**Figure 8.** Equivalent capacitance evolution

**Figure 7** and **Figure 8** are respectively, the calculated evolution of the Faradaic current density and the equivalent capacitance. At the beginning stage, due to the tiny time step caused by the initial condition, the absolute values of $J_{Far}$ and $C_{eq}$ are significant, which stabilize along the simulation process.

In order to reach the steady state of the system, the simulation needs a massive number of iterations which makes the computational cost very expensive. Moreover, reaction rates decrease significantly during the discharging process. As a consequence, the reaction event is rarely chosen, and the hopping events waste much computational capacity, which limits the simulation condition to low concentration anolyte systems.

In order to solve this problem, we have analysed several available approaches. The simplest ones are either decreasing the hopping rates manually to reduce the difference between the hopping rates and the reaction rates or deleting the hopping event completely. The former approach needs a lot of parameter testing, and the system will lose a part of its dynamics. For the latter approach, if we remove the hopping event, the discharge event can no longer occur after all the $MV^+$ inside the compact layer are discharged. Mason *et al.* suggested another approach which

eliminates all the repeating hopping events to make the displacement more effective. However, this approach is highly demanding in computational resources as well [19].

Recently, Cao *et al.* reported a fast species redistribution approach to accelerate the kMC simulations [20]. Their algorithm separates all the concerned particles into two categories: fast species which have possible fast events and slow species which only have slow events. The redistribution process is then executed as a particular operation and ensures the reasonable redistributed configuration. By implementing this particular method in the kMC algorithm, their simulation reaches longer timescales: in the immediate future, we plan to adapt this approach to our case.

# 5 Conclusions and perspectives

To conclude, this report presents our new molecular scale resolved kMC model, which aims to simulate the galvanostatic discharging process of a methyl viologen negative electrode system. This model intends to bridge the gap between the DFT calculations of WP 2 and the continuum model of WP 4.

In order to investigate the interplaying between the EDL structure and the electrochemical reactions, the model combines the VSSM algorithm with a non-equilibrium electrolyte/electrode interface EDL model reported earlier by our team [13]. The VSSM algorithm tackles the interfacial electrochemical kinetics while the EDL model simulates the electrostatic impact on discharging behaviour. The simulation captures the strong impact of the EDL on the ionic transport and electrochemical kinetics. The results of the voltage and concentration evolution demonstrate that the responses of the model to the input current density correspond to our expectations while further parameter adjustments favour the accuracy of the results.

On the other hand, our model encounters the general problem of kMC algorithms where the computational capacity is wasted mainly on uninteresting particle displacement events. There are many approaches available to solve this problem. The most promising approach is the fast species redistribution method which was recently published by Cao *et al.* [20]. For the further development of the kMC model, we intend to implement the fast species redistribution approach to save the computational cost and accomplish more target functions, such as charging process, cyclic voltammetry simulations, catholyte system simulation.

# 6 References


[1] M. Andersen, C. Panosetti, and K. Reuter, “A practical guide to surface kinetic Monte Carlo simulations,” *Front. Chem.*, vol. 7, no. APR, pp. 1–24, 2019, doi: 10.3389/fchem.2019.00202.

[2] R. A. Van Santen, *Computational Methods in Catalysis and Materials Science*. 2009.

[3] B. Andreaus and M. Eikerling, “Active site model for CO adlayer electrooxidation on nanoparticle catalysts,” *J. Electroanal. Chem.*, vol. 607, no. 1–2, pp. 121–132, 2007, doi: 10.1016/j.jelechem.2007.02.020.

[4] N. B. Luque, H. Ibach, K. Pötting, and W. Schmickler, “A simulation of two-dimensional Ostwald ripening on silver electrodes,” *Electrochim. Acta*, vol. 55, no. 19, pp. 5411–5413, 2010, doi: 10.1016/j.electacta.2010.04.066.

[5] C. Heath Turner, Z. Zhang, L. D. Gelb, and B. I. Dunlapc, “Kinetic Monte Carlo Simulation of Electrochemical Systems,” *Rev. Comput. Chem.*, vol. 28, pp. 175–204, 2015, doi: 10.1002/9781118889886.ch5.

[6] G. Shukla and A. A. Franco, “Handling Complexity of Semisolid Redox Flow Battery Operation Principles through Mechanistic Simulations,” *J. Phys. Chem. C*, vol. 122, no. 42, pp. 23867–23877, 2018, doi: 10.1021/acs.jpcc.8b06642.

[7] BIOVIA, “Materials Studio.” Dassault Systèmes, San Diego, 2015.

[8] J. Winsberg, T. Hagemann, T. Janoschka, M. D. Hager, and U. S. Schubert, “Redox-Flow Batteries: From Metals to Organic Redox-Active Materials,” *Angew. Chemie - Int. Ed.*, vol. 56, no. 3, pp. 686–711, 2017, doi: 10.1002/anie.201604925.

[9] I. Hanasaki, R. Nagura, and S. Kawano, “Coarse-grained picture of Brownian motion in water: Role of size and interaction distance range on the nature of randomness,” *J. Chem. Phys.*, vol. 142, no. 10, 2015, doi: 10.1063/1.4913748.

[10] T. Liu, X. Wei, Z. Nie, V. Sprenkle, and W. Wang, “A Total Organic Aqueous Redox Flow Battery Employing a Low Cost and Sustainable Methyl Viologen Anolyte and 4-HO-TEMPO Catholyte,” *Adv. Energy Mater.*, vol. 6, no. 3, 2016, doi: 10.1002/aenm.201501449.

[11] B. Hu, Y. Tang, J. Luo, G. Grove, Y. Guo, and T. L. Liu, “Improved radical stability of viologen anolytes in aqueous organic redox flow batteries,” *Chem. Commun.*, vol. 54, no. 50, pp. 6871–6874, 2018, doi: 10.1039/c8cc02336k.

[12] L. F. Hernández-Martínez, M. A. Chávez-Navarro, E. González-Tovar, and M. Chávez-

Páez, “A Monte Carlo study of the electrical double layer of a shape-asymmetric electrolyte around a spherical colloid,” *J. Chem. Phys.*, vol. 149, no. 16, 2018, doi: 10.1063/1.5038797.

[13] M. A. Quiroga, K.-H. Xue, T.-K. Nguyen, M. Tułodziecki, H. Huang, and A. A. Franco, “A Multiscale Model of Electrochemical Double Layers in Energy Conversion and Storage Devices,” *J. Electrochem. Soc.*, vol. 161, no. 8, pp. E3302–E3310, 2014, doi: 10.1149/2.029408jes.

[14] M. A. Quiroga and A. A. Franco, “A Multi-Paradigm Computational Model of Materials Electrochemical Reactivity for Energy Conversion and Storage,” *J. Electrochem. Soc.*, vol. 162, no. 7, pp. E73–E83, 2015, doi: 10.1149/2.1011506jes.

[15] J. P. Valleau and G. M. Torrie, “The electrical double layer. III. Modified Gouy-Chapman theory with unequal ion sizes,” *J. Chem. Phys.*, vol. 76, no. 9, pp. 4623–4630, 1982, doi: 10.1063/1.443542.

[16] A. A. Franco, P. Schott, C. Jallut, and B. Maschke, “A Dynamic Mechanistic Model of an Electrochemical Interface,” *J. Electrochem. Soc.*, vol. 153, no. 6, p. A1053, 2006, doi: 10.1149/1.2188353.

[17] P. Virtanen *et al.*, “SciPy 1.0: fundamental algorithms for scientific computing in Python,” *Nat. Methods*, vol. 17, no. 3, pp. 261–272, 2020, doi: 10.1038/s41592-019-0686-2.

[18] A. U. Modak and M. T. Lusk, “Kinetic Monte Carlo simulation of a solid-oxide fuel cell: I. Open-circuit voltage and double layer structure,” *Solid State Ionics*, vol. 176, no. 29–30, pp. 2181–2191, 2005, doi: 10.1016/j.ssi.2005.06.007.

[19] D. R. Mason, R. E. Rudd, and A. P. Sutton, “Stochastic kinetic Monte Carlo algorithms for long-range Hamiltonians,” *Comput. Phys. Commun.*, vol. 160, no. 2, pp. 140–157, 2004, doi: 10.1016/j.cpc.2004.04.002.

[20] X. M. Cao, Z. J. Shao, and P. Hu, “A fast species redistribution approach to accelerate the kinetic Monte Carlo simulation for heterogeneous catalysis,” *Phys. Chem. Chem. Phys.*, vol. 22, no. 14, pp. 7348–7364, 2020, doi: 10.1039/d0cp00554a.